Digital Equalization of Chromatic Dispersion and Polarization Mode Dispersion

Ezra Ip and Joseph M. Kahn, *Fellow, IEEE*

Abstract—In this paper, we consider a fractionally spaced equalizer (FSE) for electronic compensation of chromatic dispersion (CD) and polarization-mode dispersion (PMD) in a dually polarized (polarization-multiplexed) coherent optical communications system. Our results show that the FSE can compensate any arbitrary amount of CD and first-order PMD distortion, provided that the oversampling rate is at least 3/2 and that a sufficient number of equalizer taps are used. In contrast, the amount of CD and PMD that can be corrected by a symbol-rate equalizer only approaches an asymptotic limit, and increasing the number of taps has no effect on performance due to aliasing that causes signal cancellation and noise enhancement.

Index Terms—Chromatic dispersion (CD), coherent detection, digital signal processing, equalizers, optical fiber communication, polarization mode dispersion (PMD).

I. INTRODUCTION

CHROMATIC dispersion (CD) and polarization-mode dispersion (PMD) are two important linear distortions that affect the performance of optical systems. In traditional receivers that employ direct detection, the phase of the optical E-field is lost, making exact equalization of the channel by a linear filter impossible [1], [2]. Coherent detection circumvents this problem by combining the received signal with a local oscillator (LO) laser and by using balanced detection to downconvert it into a baseband electrical output that is proportional to the optical E-field. The resulting signal can then be sampled and processed by digital signal processing (DSP) algorithms, providing a flexible platform based on a software that is an attractive alternative to optical CD and PMD compensation [3]–[5].

In principle, any linear channel distortion can be compensated in DSP by a digital receiver operating at one sample per symbol [6]. This requires that, prior to sampling, the receiver employs an analog matched filter (matched to the convolution between the transmitted pulse shape and the channel). Also, the performance of a symbol-rate equalizer is sensitive to sampling time error. A fractionally spaced equalizer (FSE) can implement the matched filter and equalizer as a single unit and can compensate for sampling time errors, provided that the baseband signal is sampled above the Nyquist rate [6]–[9]. Thus, the FSE is widely employed in other areas of
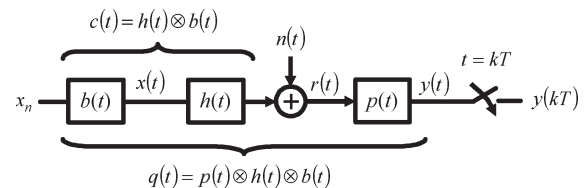
Fig. 1. Canonical model of a baseband communications channel with a digital receiver.

digital communications such as mobile radio [10] and digital subscriber lines [11]. Recent experiments in coherent optical transmission invariably use an oversampling rate of two for CD compensation [12]–[14].

In single-mode fiber (SMF) communication, PMD causes a statistical time-varying differential group delay (DGD) between the two principal states of polarization (PSP). The impact of PMD on the performance of a symbol-rate equalizer is similar to the sampling time error. Thus, it should be possible to use a polarization diversity coherent receiver in conjunction with an FSE in suppressing any arbitrary amount of PMD-induced group delay since PMD is a linear effect.

This paper is organized as follows. In Section II-A, we will review the canonical digital transmission model for a single channel and show why symbol-rate sampling is susceptible to the sampling time error and how this can be overcome by an FSE. In Section II-B, we will extend our analysis to a polarization-multiplexed optical channel. We will derive the optimal settings for a finite-length FSE and compute its mean-square error (MSE) performance. We will use the example of an SMF with CD and first-order PMD in demonstrating the ability of the FSE to compensate these distortions. In Section III, we will present numerical results and compare the performance of the symbol-rate equalizer versus the FSE. We will also compare the performance of different optical pulse shapes in the presence of CD and PMD. Further discussion is provided in Section IV.

II. THEORY

A. Canonical Digital Receiver

The canonical model of a baseband communications channel employing a digital receiver is shown in Fig. 1. The input is a set of complex-valued symbols x_n modulating a transmitted pulse shape $b(t)$. The transmission medium is assumed to be linear, having an impulse response $h(t)$, the noise added by the channel, and the receiver is modeled as $n(t)$. We denote the received pulse shape as $c(t) = h(t) \otimes b(t)$, where $\otimes$ denotes linear convolution.

The front end of the canonical digital receiver consists of a band-limiting filter whose impulse response is $p(t)$. The output $y(t)$ is then sampled at rate $1/T = M/KT_s$, where T_s is the symbol interval, and M and K are integers. For symbol-rate sampling, $M = K = 1$. We can write the sampled signal as

$$y_k \stackrel{\Delta}{=} y(kT) = \sum_n x_n q(kT - nT_s) + n'(kT) \qquad (1)$$

where $q(t) = p(t) \otimes h(t) \otimes b(t)$ is the received pulse shape after filtering, and $n' = p(t) \otimes n(t)$. If the channel's impulse response $h(t)$ is known, the optimum receiver consists of a matched filter $p(t) = c^*(-t)$,[1] followed by a symbol-rate sampler [6]. However, symbol-rate sampling has significant drawbacks. First, the exact channel impulse response may not be known. Second, it may not be possible to synthesize the analog function $c^*(-t)$ exactly. Third, a symbol-rate equalizer is sensitive to sampling time error. Consider the discrete-time Fourier transform (DTFT) of (1), where we ignore the noise term. We have

$$Y_{\text{sig}}(e^{j\omega T}) = X\left(e^{j\omega T_s}\right) \cdot \frac{1}{T} \sum_m Q\left(\omega - \frac{2\pi m}{T}\right) \qquad (2)$$

where $Q(\omega)$ is the Fourier transform of $q(t)$, and $X(e^{j\omega T_s})$ and $Y(e^{j\omega T})$ are the DTFTs of the sequences x_k and y_k, respectively. The zero-forcing (ZF) linear filter that can undo the channel's distortion has a DTFT given by the following:

$$W_{\text{ZF}}(e^{j\omega T}) = \left[1/T \sum_m Q\left(\omega - 2\pi m/T\right)\right]^{-1}. \qquad (3)$$

However, in the presence of a sampling delay τ_s, the sampled sequence becomes $y'_k = y(kT - \tau_s)$. We can characterize the impact on the system by defining the postfiltered pulse shape as $q'(t) = q(t - \tau_s)$. The DTFT of the signal term becomes

$$Y'_{\text{sig}}(e^{j\omega T}) = X(e^{j\omega T_s}) \cdot \frac{1}{T} \sum_m Q\left(\omega - \frac{2\pi m}{T}\right) e^{-j\left(\omega - \frac{2\pi m}{T}\right)\tau_s}. \qquad (4)$$

In comparison with (2), each term in the summation over m is multiplied by a phase shift. If sampling is performed below the Nyquist rate, spectral overlap between the $Q(\omega - 2\pi m/T)\exp(-j(\omega - 2\pi m/T)\tau_s)$ terms will occur. It is possible that, for some values of τ_s, the phase shift will cause the overlapping spectra to interfere destructively, leading to signal cancellation. Even if the equalizer is designed according to the minimum MSE (MMSE) criteria, noise enhancement will still happen. A digital receiver that employs sub-Nyquist-rate sampling is therefore susceptible to sampling time errors. This problem is particularly acute when symbol-rate sampling is used because spectral overlap always occurs, unless $q(t)$ is a sinc function, which is not realizable in practice.

---

[1]Throughout this paper, we shall use superscripts *, $^\text{T}$, and $^\text{H}$ in denoting the complex conjugate, the transpose, and the Hermitian transpose of matrix variables, respectively. A scalar is simply a special case of a 1×1 matrix.
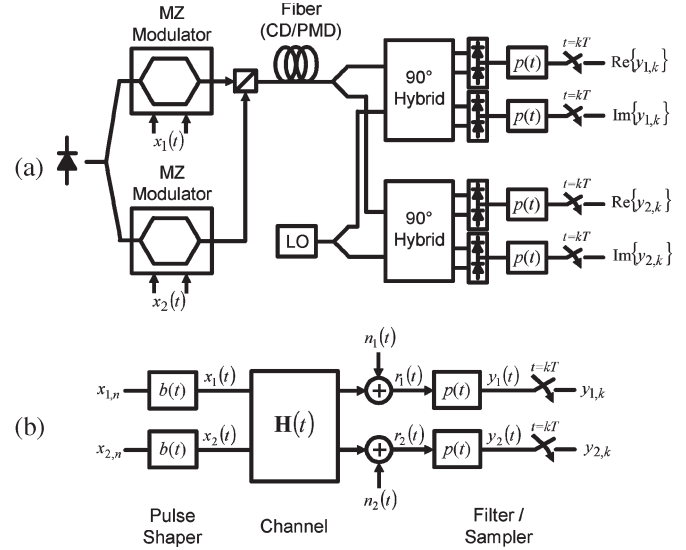

Fig. 2. (a) Dual-polarization coherent optical system employing homodyne detection. (b) Equivalent baseband model.

B. Polarization-Diversity Receiver

The canonical model of a dual-polarization (polarization-multiplexed) coherent optical system employing a homodyne receiver is shown in Fig. 2(a). The transmitter consists of two Mach–Zehnder (MZ) modulators, where each modulator is capable of generating symbols from any arbitrary signal constellation [15]. The two optical data streams, which are polarized in orthogonal directions, are then combined using a polarization beam splitter. After passing through an SMF, the received signal is split into two paths that are mixed with the LO through a network consisting of two 90° hybrids and, then, is coherently detected using four balanced photodetectors. The electrical outputs are baseband signals corresponding to the I and Q associated with the polarizations parallel and orthogonal to the LO. These signals are then passed through low-pass antialiasing filters having an impulse response $p(t)$ and are sampled at a rate of $1/T$ using analog-to-digital converters (ADCs).

The dual-polarization coherent receiver has a baseband equivalent model that is shown in Fig. 2(b). The transmitted signals in the two input polarizations are of the form

$$x_j(t) = \sum_n x_{j,n} b(t - nT_s) \qquad (5)$$

where $x_{j,n}$ is the nth symbol transmitted in the jth polarization of the fiber, and $b(t)$ is the transmitted pulse shape, which is assumed to be the same for both channels. We can also write the transmitted signal in vector notation as $\mathbf{x}(t) = [x_1(t), x_2(t)]^\text{T}$. The received signal is then expressed as

$$\mathbf{r}(t) = \mathbf{h}(t) \otimes \mathbf{x}(t) + \mathbf{n}(t) \qquad (6)$$

where

$$\mathbf{h}(t) = \begin{bmatrix} \mathbf{h}_{11}(t) & \mathbf{h}_{12}(t) \\ \mathbf{h}_{21}(t) & \mathbf{h}_{22}(t) \end{bmatrix}. \qquad (7)$$

$\mathbf{h}(t)$ is the matrix representation of the fiber impulse response, where $h_{ij}(t)$ denotes the response of the ith output polarization to an impulse in the jth input polarization. $\mathbf{n}(t) = [n_1(t), n_2(t)]^{\mathrm{T}}$ and $\mathbf{r}(t) = [r_1(t), r_2(t)]^{\mathrm{T}}$ are the noise and the received signal vectors, respectively.

We note that (7) is a complete description of any dually polarized linear channel and can characterize both CD and any order of PMD. For instance, the frequency response $\mathbf{H}(\omega) = \mathbf{F}\{\mathbf{h}(t)\}$ of an SMF with CD and first-order PMD has the form

$$\mathbf{H}(\omega) = \begin{bmatrix} \cos\theta & -\sin\theta \\ \sin\theta & \cos\theta \end{bmatrix} \begin{bmatrix} e^{j\omega\tau/2} & 0 \\ 0 & e^{-j\omega\tau/2} \end{bmatrix}$$
$$\times \begin{bmatrix} \cos\theta & \sin\theta \\ -\sin\theta & \cos\theta \end{bmatrix} \times e^{-j\frac{1}{2}\beta_2 L_{\mathrm{fiber}}\omega^2} \quad (8)$$

where β_2 is the fiber's GVD parameter [16], L_{fiber} is the fiber length, θ is the angle between the reference polarizations and the PSP of the fiber, and τ is the DGD between the PSPs.

In this paper, we shall assume that all fiber nonlinear effects, as well as the phase noises of the transmitter and LO lasers, are either negligible or compensated so that the fiber can be modeled as a linear channel. The baseband electrical signals recovered by the polarization-diversity receiver are expressed as

$$r_i(t) = \sum_n \sum_{j=1}^2 x_{j,n} c_{ij}(t - nT_s) + n_i(t) \quad (9)$$

where $c_{ij}(t) = h_{ij}(t) \otimes b(t)$, and $n_i(t)$ is an additive white Gaussian noise (AWGN)[2] process with two-sided power-spectral density (psd) of N_0.

Upon passing $r_i(t)$ through $p(t)$, the sampled outputs are

$$y_i(kT) \triangleq y_{i,k} = \sum_n \sum_{j=1}^2 x_{j,n} q_{ij}(kT - nT_s) + n_i'(kT) \quad (10)$$

where $q_{ij}(t) = p(t) \otimes h_{ij}(t) \otimes b(t)$, and $n_i' = p(t) \otimes n_i(t)$.

We now derive the optimal coefficients for a linear transversal filter $\mathbf{W}$ whose output is an MMSE estimates of the transmitted symbols. The equalizer computes

$$\hat{\mathbf{x}}_k = \begin{bmatrix} \hat{x}_{1,k} \\ \hat{x}_{2,k} \end{bmatrix} = \begin{bmatrix} \mathbf{W}_{11}^{\mathrm{T}} & \mathbf{W}_{21}^{\mathrm{T}} \\ \mathbf{W}_{12}^{\mathrm{T}} & \mathbf{W}_{22}^{\mathrm{T}} \end{bmatrix} \begin{bmatrix} \mathbf{y}_{1,k} \\ \mathbf{y}_{2,k} \end{bmatrix} = \mathbf{W}^{\mathrm{T}} \mathbf{y}_k \quad (11)$$

where $\mathbf{y}_{i,k} = \lfloor y_{i,\lfloor kM/K \rfloor + L}, \ y_{i, \lfloor kM/K \rfloor + L-1}, \ \cdots, \ y_{i,\lfloor kM/K \rfloor - L} \rfloor^{\mathrm{T}}$, and $\mathbf{W}_{ij} = [W_{ij,-L}, W_{ij,-L+1}, \ldots, W_{ij,L}]^{\mathrm{T}}$ are column vectors of length $N = 2L + 1$, and $\lfloor x \rfloor$ denotes the largest integer less than or equal to x. It can be shown that the Wiener filter coefficients are given by the following:

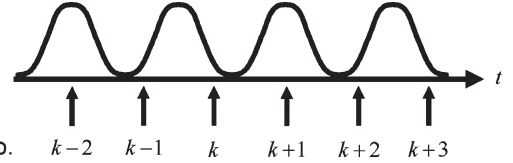$$\mathbf{W}_{\mathrm{opt}} = \mathbf{A}^{-1} \alpha \quad (12)$$

Fig. 3. For noninteger oversampling, the sample times relative to the symbol peaks differ between neighboring symbols. In the 3/2-oversampling example shown, odd symbols have a sample near the optimum sampling instant, whereas even symbols have two samples straddling the symbol peak.

where $\mathbf{A} = E\lfloor \mathbf{y}_k^* \mathbf{y}_k^{\mathrm{T}} \rfloor$, and $\alpha = E\lfloor \mathbf{y}_k^* \mathbf{x}_k^{\mathrm{T}} \rfloor$. We can partition these matrices as

$$\mathbf{A} = \begin{bmatrix} \mathbf{A}_{11} & \mathbf{A}_{12} \\ \mathbf{A}_{21} & \mathbf{A}_{22} \end{bmatrix} \quad (13)$$

and

$$\boldsymbol{\alpha} = \begin{bmatrix} \boldsymbol{\alpha}_{11} & \boldsymbol{\alpha}_{12} \\ \boldsymbol{\alpha}_{21} & \boldsymbol{\alpha}_{22} \end{bmatrix}. \quad (14)$$

The submatrices $\mathbf{A}_{ij} = E\lfloor \mathbf{y}_{i,k}^* \mathbf{y}_{j,k}^{\mathrm{T}} \rfloor$ are $N \times N$, whereas the column vectors $\boldsymbol{\alpha}_{ij} = E\lfloor \mathbf{y}_{i,k}^* x_{j,k} \rfloor$ are of length N. Let $\mathbf{A}_{ij,lm}$ be the element at the intersection of the lth row and mth column of submatrix $\mathbf{A}_{ij}$. Similarly, let $\boldsymbol{\alpha}_{ij,l}$ be the element at the lth row of $\boldsymbol{\alpha}_{ij}$. By assuming that the transmitted symbols are independent identically distributed (i.i.d.), satisfying $E\lfloor x_{i,l} x_{j,m}^* \rfloor = P_x \delta_{ijlm}$, we have

$$\mathbf{A}_{ij,lm} = P_x \sum_n \sum_{s=1}^2 q_{is}^* \left(\left\lfloor \frac{kM}{K} \right\rfloor T - lT - nT_s \right) q_{js}$$
$$\times \left(\left\lfloor \frac{kM}{K} \right\rfloor T - mT - nT_s \right)$$
$$+ N_0 \int_{-\infty}^{+\infty} p^*(t - lT) p(t - mT) dt \quad (15)$$

and

$$\boldsymbol{\alpha}_{ij,l} = P_x \sum_{s=1}^2 q_{is}^* \left(\left\lfloor \frac{kM}{K} \right\rfloor T - lT - kT_s \right). \quad (16)$$

We observed that (15) and (16) can take on K different values, depending on $\mathrm{mod}(kM, K)$. This effect is shown in Fig. 3 for the case of 3/2 sampling. It is observed that the sampling time relative to the symbol peak differs for odd and even symbols. Hence, the Wiener filter that reconstructs the best estimate of the kth transmitted symbol needs to have different coefficients for k even and for k −odd. In general, a rate − M/K system needs to have K different sets of coefficients for W_{opt}. These are obtained by evaluating (15) and (16) for all possible values of $\mathrm{mod}(kM, K)$ and by substituting into (12).

A block diagram implementation of the FSE is shown in Fig. 4(a). The inputs $y_{1,n}$ and $y_{2,n}$ are the outputs of Fig. 2(b), which were sampled at intervals of $T = KT_s/M$. The W_{ij} function blocks takes $N = 2L + 1$ consecutive samples of $y_{1,k}$
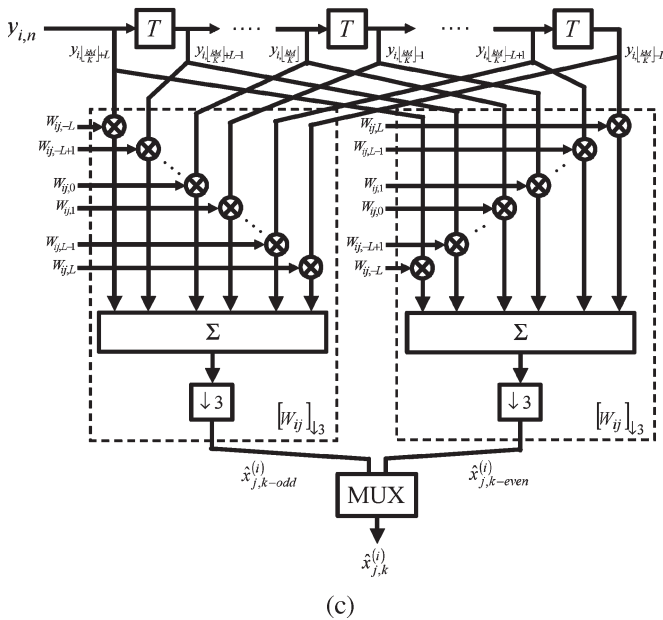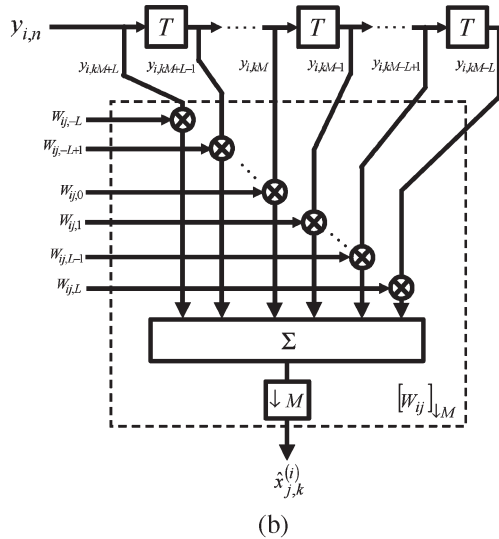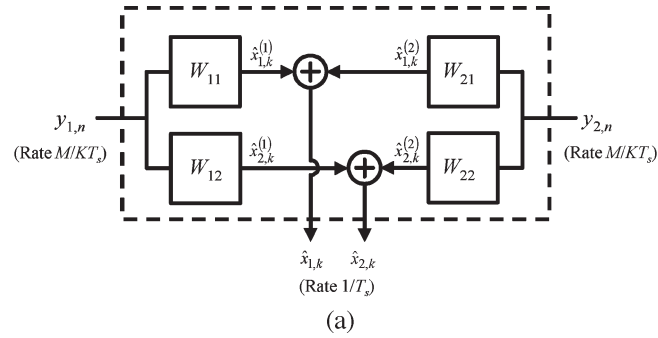
(a)

(b)

(c)

Fig. 4. (a) Block diagram of the FSE. The four signal processing blocks each implement the dot product between a compartment W_{ij} of the FSE matrix with a block of $N = 2L + 1$ samples of $y_{1,k}$ or $y_{2,k}$. The implementations of these are shown for FSEs having an oversampling rate of (b) $M/K = N$ and (c) $M/K = 3/2$.

or $y_{2,k}$ and evaluates the matrix multiplication in (11). We can implement the W_{ij} function blocks using Fig. 4(b) and (c) for the cases where the FSE has an integer oversampling rate of M and for $M/K = 3/2$. Since the FSE only needs to produce an output at the symbol rate $1/T_s$, the concatenation of the

finite impulse response (FIR) filter, followed by decimation (the dashed boxes $[W_{ij}]_{\downarrow M}$), can, in fact, be implemented by a polyphase filter. Let $\varepsilon_k = \mathbf{x}_k - \hat{\mathbf{x}}_k$ be the error between the transmitted symbols and the output of the FSE in (11). It is shown that using the Wiener filter coefficients for the FSE results in the MSE matrix

$$E\lfloor \varepsilon_k \varepsilon_k^{\mathrm{H}} \rfloor = P_x \mathbf{I} - \boldsymbol{\alpha}^{\mathrm{H}} \mathbf{A}^{-1} \boldsymbol{\alpha}. \tag{17}$$

We then have

$$\mathrm{MSE}_{\mathrm{MMSE}} = \sum_{s=1}^{2} E\left[|\varepsilon_{s,k}|^2 \right] = \mathrm{tr} E\left[\varepsilon_k \varepsilon_k^{\mathrm{H}} \right]. \tag{18}$$

For an oversampling rate of M/K, where $K \neq 1$, (17) needs to be averaged over all K phases of (15) and (16).

1) Limiting Performance of the FSE: In the limit where the rate of the FSE $1/T = M/KT_s$ satisfies the Nyquist's criterion, the frequency range $|\omega| < \pi/T$ bears all the information in the analog received signal. We can write (10) in terms of its DTFT as

$$\mathbf{Y} = \mathbf{QX} + \mathbf{N}'. \tag{19}$$

For convenience, we have dropped the $e^{j\omega T}$ in our DTFTs. The error between the transmitted symbols and the FSE output is

$$\boldsymbol{\varepsilon} = \mathbf{X} - \mathbf{W}^{\mathrm{T}} \mathbf{Y} = (\mathbf{I} - \mathbf{W}^{\mathrm{T}} \mathbf{Q}) \mathbf{X} - \mathbf{W}^{\mathrm{T}} \mathbf{N}'. \tag{20}$$

We can write $\mathbf{Q}$ in terms of its singular value decomposition $\mathbf{Q} = \mathbf{U} \mathbf{S} \mathbf{V}^{\mathrm{H}}$. If the symbols are i.i.d., satisfying $E\lfloor x_{i,l} x_{j,m}^* \rfloor = P_x \delta_{ijlm}$, the MSE matrix is given by the following:

$$
\begin{aligned}
E[\varepsilon \varepsilon^{\mathrm{H}}] =\ & \left(\mathbf{W}^{\mathrm{T}} \mathbf{U} - P_x \mathbf{V} \mathbf{S} \left(P_x \mathbf{S}^2 + S_{N'N'} \mathbf{I} \right)^{-1} \right) \\
& \times \left(P_x \mathbf{S}^2 + S_{N'N'} \mathbf{I} \right) \\
& \times \left(\mathbf{W}^{\mathrm{T}} \mathbf{U} - P_x \mathbf{V} \mathbf{S} \left(P_x \mathbf{S}^2 + S_{N'N'} \mathbf{I} \right)^{-1} \right)^{\mathrm{H}} \\
& + \left(P_x - P_x^2 \mathbf{V} \mathbf{S} \left(P_x \mathbf{S}^2 + S_{N'N'} \mathbf{I} \right)^{-1} \mathbf{S} \mathbf{V}^{\mathrm{H}} \right)
\end{aligned}
\tag{21}
$$

where the psd of the filtered noise is

$$S_{N'N'}(e^{j\omega T}) = N_0 \frac{1}{T} \sum_m \left| P\left(\omega - \frac{2\pi m}{T} \right) \right|^2. \tag{22}$$

The goal of $\mathbf{W}$ is to minimize $\mathrm{tr} E[\varepsilon \varepsilon^{\mathrm{H}}]$, which is equal to the sum of the eigenvalues of (21). Since $(P_x \mathbf{S}^2 + S_{N'N'} \mathbf{I})$ is positive definite, (21) is minimized by setting its first term to zero. Thus, we have

$$\mathbf{W}_{\mathrm{opt}}^{\mathrm{T}} = P_x \mathbf{V} \mathbf{S} \left(P_x \mathbf{S}^2 + S_{N'N'} \mathbf{I} \right)^{-1} \mathbf{U}^{\mathrm{H}}. \tag{23}$$

We note that the Wiener solution given in (23) is a function of frequency. The FSE coefficients may be found by taking the inverse DTFT

$$\mathbf{w}_{\text{opt},n} = \frac{T}{2\pi} \int_{-\pi/T}^{\pi/T} \mathbf{W}_{\text{opt}} \left(e^{j\omega T}\right) e^{j\omega nT} d\omega. \qquad (24)$$

The psd of the resulting MSE is then equal to the sum of the eigenvalues of the second term of (21). By using Parseval's theorem, we have

$$\text{MSE}_{\text{MMSE}} = \sum_{i=1}^{2} E \left[|\varepsilon_{i,k}|^2 \right]$$

$$= \frac{T}{2\pi} \int_{-\pi/T}^{\pi/T} \sum_{i=1}^{2} \frac{P_x S_{N'N'}(e^{j\omega T})}{P_x s_i^2(e^{j\omega T}) + S_{N'N'}(e^{j\omega T})} d\omega \qquad (25)$$

where $s_i(e^{j\omega T})$ is the frequency-dependent singular value of $\mathbf{Q}(e^{j\omega T})$.

2) CD/PMD Example: To see that the Wiener solution in (23) is indeed optimal, consider the fiber channel given in (8). Since $b(t)$ and $p(t)$ are identical for the two polarizations, we have $\mathbf{Q}(e^{j\omega T}) = P(e^{j\omega T})B(e^{j\omega T})\mathbf{H}(e^{j\omega T})$. As $\mathbf{H}$ has unit singular values, we have $s_i^2(e^{j\omega T}) = |P(e^{j\omega T})B(e^{j\omega T})|^2 = |Q(e^{j\omega T})|^2$, for $i = 1$ and 2. Therefore

$$\mathbf{W}_{\text{opt}}^T(e^{j\omega T}) = \frac{P_x Q(e^{j\omega T})}{P_x |Q(e^{j\omega T})|^2 + S_{N'N'}(e^{j\omega T})} \mathbf{H}^*(e^{j\omega T}) \qquad (26)$$

where we note that

$$\mathbf{H}^*(e^{j\omega T}) = \begin{bmatrix} \cos\theta & -\sin\theta \\ \sin\theta & \cos\theta \end{bmatrix} \begin{bmatrix} e^{-j\omega\tau/2} & 0 \\ 0 & e^{j\omega\tau/2} \end{bmatrix}$$

$$\times \begin{bmatrix} \cos\theta & \sin\theta \\ -\sin\theta & \cos\theta \end{bmatrix} \times e^{j\frac{1}{2}\beta_2 L_{\text{fiber}}\omega^2}. \qquad (27)$$

It is the filter that exactly cancels the CD and first-order PMD of the channel over the frequency range $|\omega| < \pi/T$. The scaling factor in (25) is an artifact of minimizing MSE [17]. If the system is symmetric, we can define the unbiased SNR for the FSE output as

$$\text{SNR}_{\text{MMSE}-U} = \frac{2P_x}{\text{MSE}_{\text{MMSE}}} - 1. \qquad (28)$$

Finally, we define the input SNR per symbol to be

$$\text{SNR}_{\text{in}} = \frac{P_x T_s}{N_0} = \frac{E_s}{N_0}. \qquad (29)$$

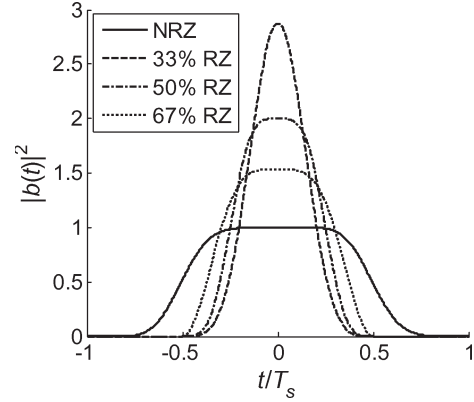The ratio between (29) and (28) is the system power penalty.

Fig. 5. Intensity waveforms of isolated NRZ, 33% RZ, 50% RZ, and 67% RZ pulses. Normalized pulses are shown with unit energy.

III. NUMERICAL RESULTS

We simulated the performances of the symbol-rate equalizer and the FSE for four commonly used optical pulse shapes. These are the nonreturn to zero (NRZ), 33% RZ, 50% RZ, and 67% RZ pulses. The analytical formulas for the RZ pulses and their respective spectra were studied in [18]. For NRZ [19], we assumed that the electrical drive signals for the MZ modulator were produced by passing an ideal rectangular pulse train through a fifth-order low-pass Bessel filter with a 3-dB bandwidth of $0.8/T_s$. The normalized waveforms of these pulses are shown in Fig. 5. For the receiver, we assumed that the antialiasing filter $p(t)$ is a fifth order of any of the following: 1) Bessel filter or 2) Butterworth filter with a 3-dB bandwidth of $0.4/T$, where $1/T = M/KT_s$ is the sampling rate. We shall compare the relative performances of the choices of $p(t)$.

In Figs. 6 and 7, we show the amount of CD that a symbol-rate equalizer and an FSE with N taps (corresponding to $\mathbf{W}$ being of size $2N \times 2$) can tolerate with less than 2-dB power penalty at an input SNR of 20 dB per symbol, as defined by (28) and (29). Figs. 6 and 7 consider Bessel and Butterworth filters, respectively. We observed that, while the correctable amount of CD grows almost linearly with N for the FSE, the result for the symbol-rate equalizer only approaches an asymptote. This is due to the effect of aliasing that was described in Section II-A, where signal cancellation by the overlapping spectra leads to noise enhancement. The effect of aliasing is also apparent for an FSE with 3/2 times oversampling when 33% and 50% RZs are used in conjunction with a Bessel filter. This is because 33% and 50% RZs have a higher proportion of its energy outside $|\omega| < \pi/T$. The Bessel filter, with its gradual roll-off, is less able to prevent aliasing. In contrast, the Butterworth filter can better suppress the received signal's sidelobes. Even though the Butterworth filter does not have a linear phase, its phase distortion is corrected by the FSE. Hence, the Butterworth filter achieves superior performance at low oversampling. Since the sampling rate of ADCs is often a limiting factor in current coherent optical systems,[3] the reduced oversampling requirement can be of significance. For FSEs operating at $M/K \geq 2$, the CD performance of all pulse shapes

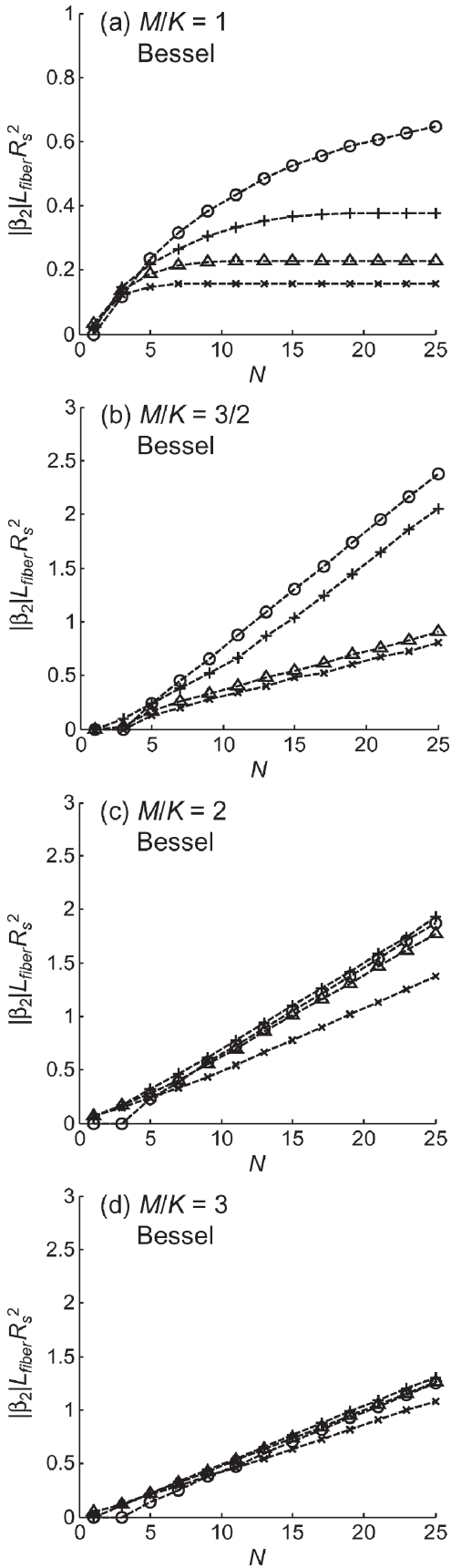[3]The fastest ADC commercially available in April 2007 is around 20 GSa/s.

Fig. 6. Maximum allowable CD versus the number of equalizer taps for a 2-dB power penalty at an input SNR of 20 dB per symbol, using a Bessel antialiasing filter. "o" denotes transmission using NRZ pulses, "x" denotes 33% RZ, "Δ" denotes 50% RZ, and "$+$" denotes 67% RZ.
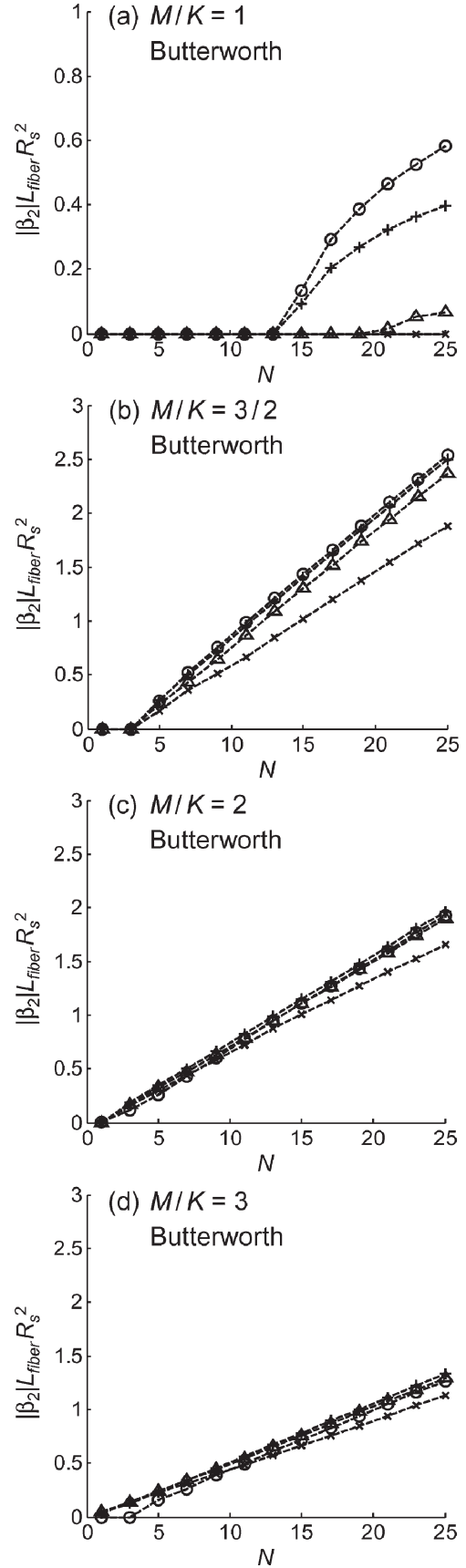
Fig. 7. Maximum allowable CD versus the number of equalizer taps for a 2-dB power penalty at an input SNR of 20 dB per symbol, using a Butterworth antialiasing filter. "o" denotes transmission using NRZ pulses, "x" denotes 33% RZ, "Δ" denotes 50% RZ, and "$+$" denotes 67% RZ.

is similar, regardless of whether a Bessel or Butterworth filter is used.

The linearity between CD and the FSE length is intuitively satisfying since the delay difference between two packets of energy that are separated by $\Delta\omega$ in frequency is given by $\tau_{DD} = |\beta_2|L_{\text{fiber}}\Delta\omega$. As the bandwidth of the transmitted signal is proportional to R_s, we expect that the pulse spreading will assume the form $\tau_{DD} \propto 2\pi|\beta_2|L_{\text{fiber}}R_s$, which corresponds to $N_{DD} \propto 2\pi|\beta_2|L_{\text{fiber}}R_s^2(M/K)$ sampling intervals. In order to cancel the intersymbol interference (ISI) of a $q(t)$ that has a significant energy over N_{DD} samples, we expect $N \propto N_{DD}$ taps are needed. Fig. 6(c) and (d) and Fig. 7(b)–(d) confirm the linearity between $|\beta_2|L_{\text{fiber}}R_s^2$ and N, where the empirical relationship is

$$|\beta_2|L_{\text{fiber}}R_s^2\,(M/K) \approx 0.15N. \qquad (30)$$

This formula is consistent with the results of the study in [20], which considered rounded pulses with 35% excess bandwidth and an FSE with $M/K = 2$.

In Figs. 8 and 9, the performance of the symbol-rate equalizer and the FSE in the presence of a first-order PMD is shown. Figs. 8 and 9 consider Bessel and Butterworth filters, respectively. We assume that the fiber has no CD, and the angle between the input signal polarizations and the PSP is $\theta = 45°$ (worst case). Again, the correctable amount of PMD approaches asymptotic limits for the symbol-rate equalizer, whereas for the FSE, the tolerable τ grows linearly with N. This is, again, intuitively satisfying since a PMD channel with a DGD of τ will have an impulse response consisting of two peaks separated by $N = \tau M/KT_s$ samples. This matches the slopes observed in Figs. 8(b)–(d) and 9(b)–(d).

The required filter length will typically be dictated by CD, not by PMD. Pulse spreading that is caused by PMD is typically less than one symbol interval, while that caused by CD typically spans several symbol intervals. For example, consider a symbol rate $R_s = 10$ GHz and a fiber of length $L_{\text{fiber}} = 2000$ km having a PMD of 0.1 ps/$\sqrt{\text{km}}$ and a CD of 17 ps/(nm $\cdot$ km). By considering PMD, the mean DGD is $\bar{\tau} = 4.5$ ps, and a DGD of five times the mean corresponds to $\tau/T_s = 0.22$ symbol intervals. Suppose the CD is compensated to within 5% error, corresponding to an uncompensated length $L_{\text{fiber}} = 100$ km. We have $2\pi|\beta_2|L_{\text{fiber}}R_s^2 = 8.5$ symbol intervals. Thus, setting N to the value given by (30) is typically more than enough to compensate PMD. The combined power penalty from both effects should be close to 2 dB, which is caused almost entirely by CD.

To illustrate the tolerance of an FSE to sampling time error, we plot the MSE per channel versus τ_s/T_s in Figs. 10 and 11, assuming no CD or PMD. Figs. 10 and 11 consider Bessel and Butterworth filters, respectively. The input SNR per symbol is 20 dB. As expected, we observed performance degradation for the symbol-rate sampler. Although some noise enhancement is present for the FSE with 3/2 times oversampling, the MSE becomes insensitive to sampling time error for $M/K \geq 2$.

Finally, we recall that our theoretical analysis and simulation results used MSE as the criterion for evaluating system performance. In practice, MSE incorporates the effects of AWGN,
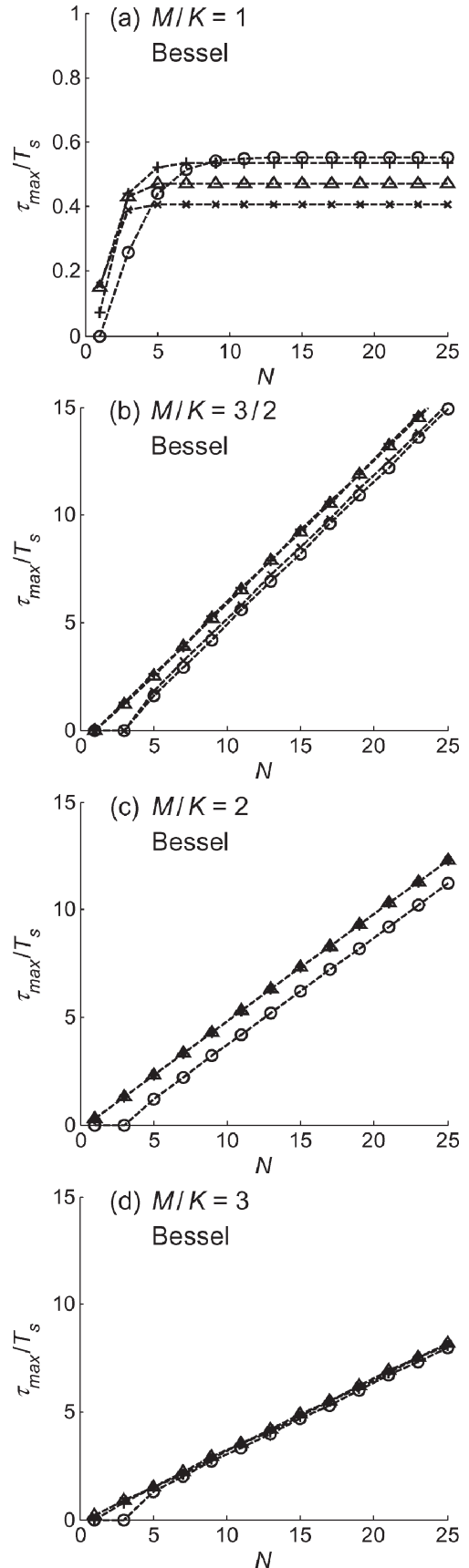

Fig. 8.   Maximum allowable PMD DGD versus the number of equalizer taps for a 2-dB power penalty at an input SNR of 20 dB per symbol using a Bessel antialiasing filter. "o" denotes transmission using NRZ pulses, "x" denotes 33% RZ, "Δ" denotes 50% RZ, and "$+$" denotes 67% RZ.
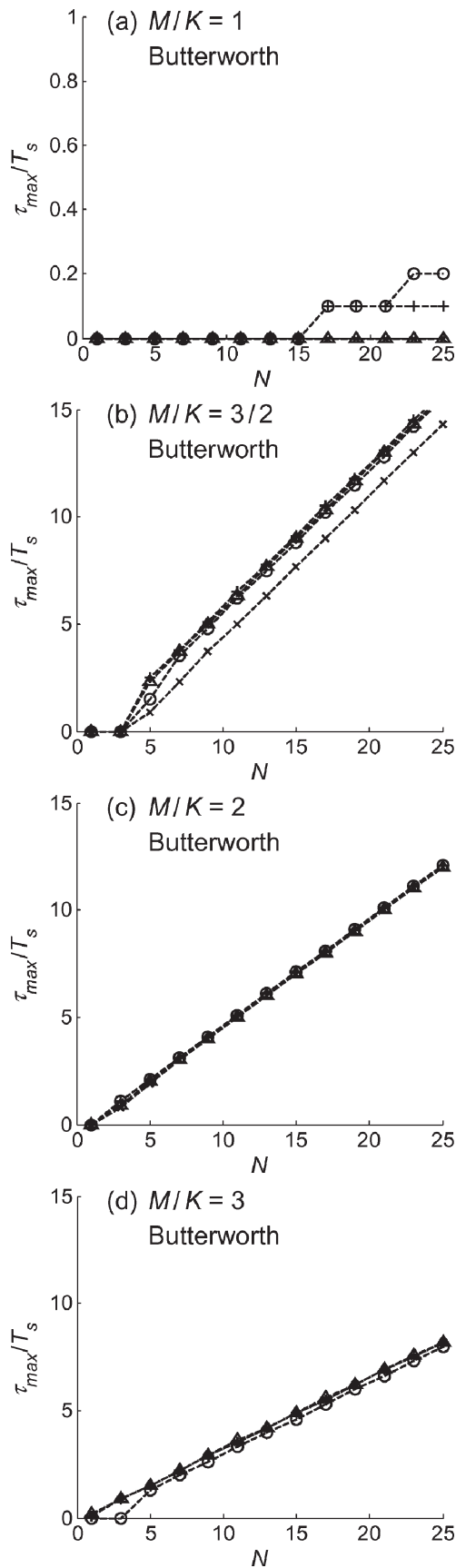
Fig. 9. Maximum allowable PMD DGD versus the number of equalizer taps for a 2-dB power penalty at an input SNR of 20 dB per symbol using a Butterworth antialiasing filter. "o" denotes transmission using NRZ pulses, "x" denotes 33% RZ, "Δ" denotes 50% RZ, and "$+$" denotes 67% RZ.

Fig. 10. MSE at the output of the digital equalizer versus the sampling time delay for a channel with no CD or PMD at an input SNR of 20 dB per symbol using a Bessel antialiasing filter. "o" denotes transmission using NRZ pulses, "x" denotes 33% RZ, "Δ" denotes 50% RZ, and "$+$" denotes 67% RZ.
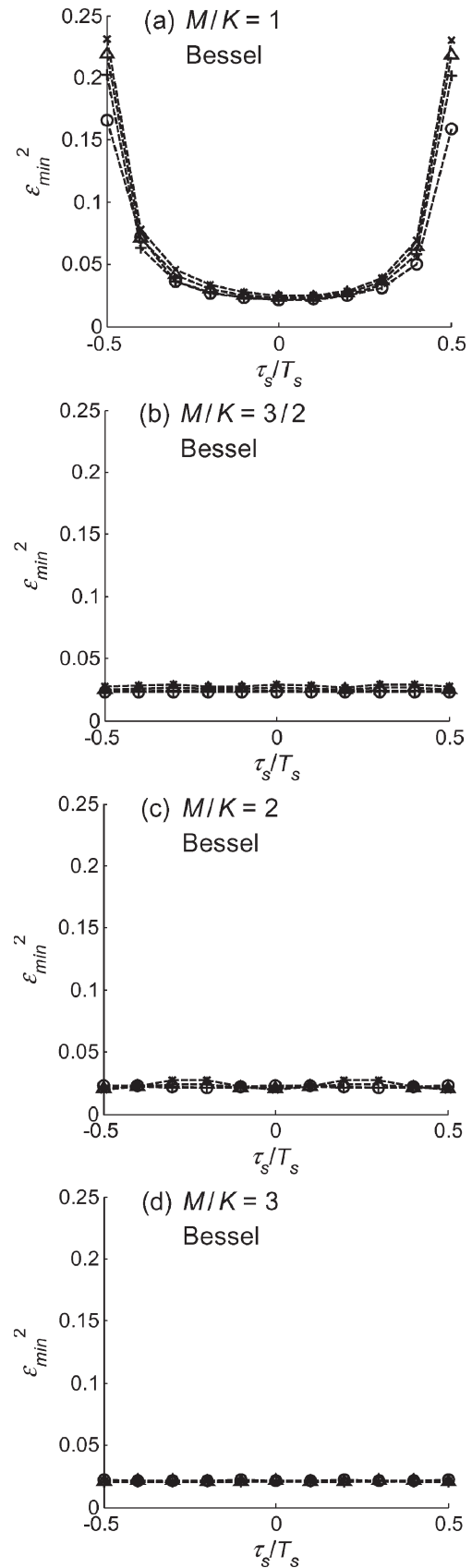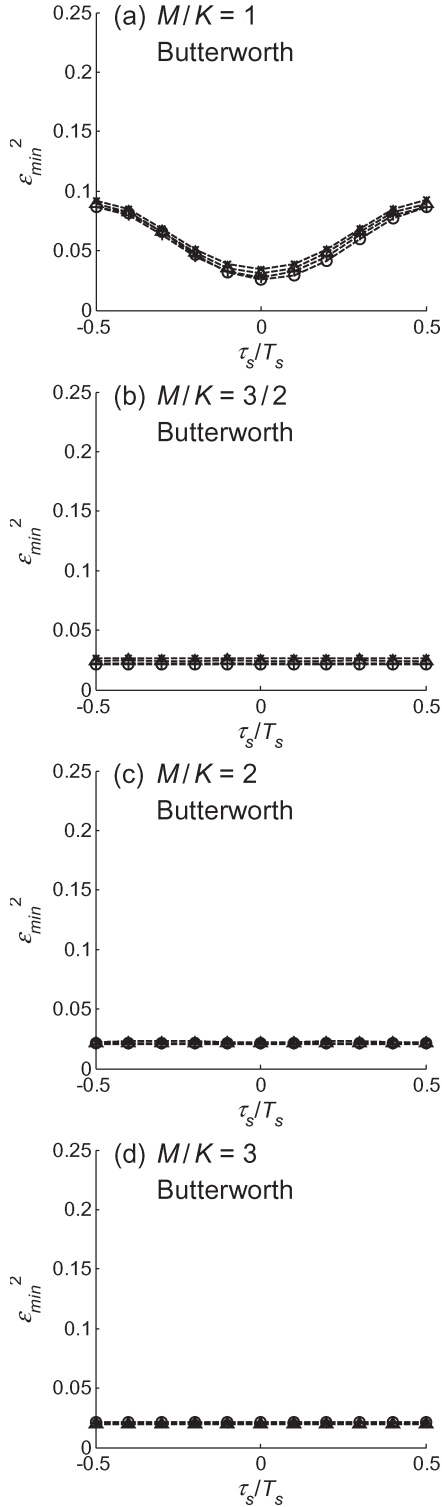
Fig. 11. MSE at the output of the digital equalizer versus the sampling time delay for a channel with no CD or PMD at an input SNR of 20 dB per symbol using a Butterworth antialiasing filter. "o" denotes transmission using NRZ pulses, "x" denotes 33% RZ, "$\triangle$" denotes 50% RZ, and "$+$" denotes 67% RZ.
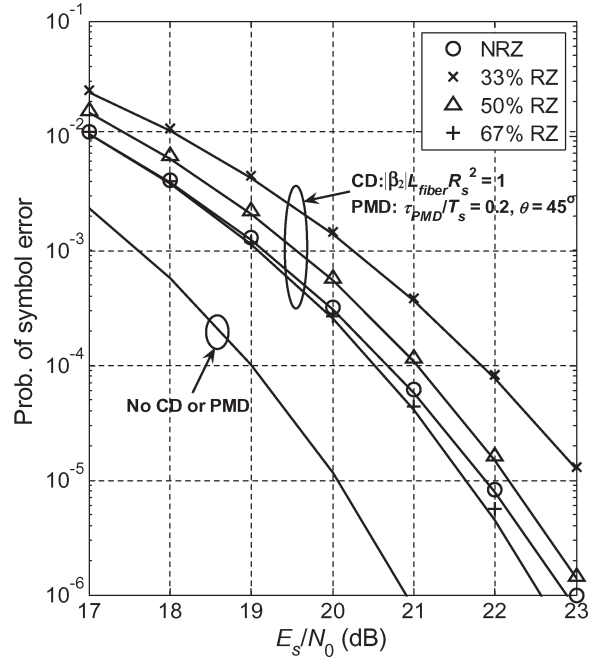

Fig. 12. Probability of symbol error versus input SNR per symbol for a 16-QAM transmission over an optical channel with CD and first-order PMD, with the receiver employing an FSE with 15 taps at an oversampling rate of $M/K = 2$. "o" denotes Monte Carlo simulation results for NRZ transmission, "x" denotes 33% RZ, "$\triangle$" denotes 50% RZ, and "$+$" denotes 67% RZ. The solid lines are theoretical SER curves, assuming that the error signal after digital equalization is Gaussian-distributed.

ISI, and crosstalk between the two polarization-multiplexed channels. The ultimate parameter of interest is the system bit-error ratio (BER). However, optimization of the FSE with respect to BER leads to intractable equations; hence, MMSE is the most widely used criterion. A potential flaw of the MSE approach is that ISI and crosstalk may not have Gaussian statistics, as it is unlikely that the residual impulse duration after equalization is long enough for these effects to achieve Gaussianity. Thus, the actual BER of the system may not be the same as the one expected for a system with the output SNR defined in (28).

To show that the MSE characterization is valid, we plot the symbol error rate (SER) against the input SNR per symbol for a channel with a CD of $|\beta_2|L_{fiber}R_s^2 = 1$ and a PMD group delay of $\tau = T_s/5$, where the PSP angle is 45°. We assumed $p(t)$ to be a fifth-order Bessel filter with a 3-dB bandwidth of $0.4/T$. Our simulation used 16-QAM transmission with $N = 15$ taps. From Fig. 6, we expect the system to have power penalties around 2 dB. Fig. 12 shows the SER obtained by Monte Carlo simulations as well as the theoretical SER (solid curves) for Gaussian noise

$$\text{SER}_{QAM-16} = \frac{3}{2}\text{erfc}\left(\sqrt{\frac{\text{SNR}_{MMSE-U}}{10}}\right). \qquad (31)$$

The agreement between the Monte Carlo simulations and the theoretical SER formula shows that the MMSE criterion is valid.

IV. DISCUSSION

In this paper, we have only considered fixed equalizer taps for the FSE. In practice, it is possible—and often desirable—to implement $\mathbf{W}$ as an adaptive filter. Such an approach is useful when the exact frequency response of the channel is not known.

TABLE I
OSNR REQUIREMENT FOR VARIOUS MODULATION FORMATS

Modulation Format	SNR per symbol required for a target BER of 10^{-3}
4-QAM	9.80 dB
8-QAM	13.80 dB
16-QAM	16.54 dB

In particular, PMD is statistically time varying, so that an adaptive algorithm allows **W** to continually adjust for the best MSE performance. Since the system is linear and we have shown that the MSE performance in (21) surface is parabolic, we expect an adaptive solution to be well behaved.

In terms of implementing the FSE, there are two key considerations: the number of bits required for the ADCs and the system complexity. Table I shows the optical signal-to-noise ratio (OSNR) per symbol required for 4-, 8-, and 16-QAM transmissions. Suppose we allow a 2-dB power penalty for CD/PMD compensation and a 1.5-dB margin for other impairments. A 16-QAM requires an OSNR of 20 dB. ADC quantization adds noise with variance $\Delta^2/12$ per sample, where Δ is the quantization step size. Suppose we require quantization noise variance to be less than 10% of the AWGN variance per dimension, which is $N_0/2T = N_0 M/2KT_s$. For $M/K = 3/2$, this gives $\Delta < 0.095\sqrt{P_x}$, where P_x is the transmitted power. To determine the output range of the required ADC, we note that the outermost symbols in 16-QAM have a magnitude of $3\sqrt{P_x/10} = 0.95\sqrt{P_x}$ per dimension, and from Fig. 3, the peak amplitude of a unit energy 33%-RZ pulse is less than three. Hence, even for the worst case of 33%-RZ 16-QAM transmission, the ADC output only needs to swing between $\pm2.85\sqrt{P_x}$, corresponding to 60 Δ. Even when allowing for amplitude distortion due to CD/PMD distortion, an 8-b resolution should be more than sufficient.

To determine the system complexity, consider the example in Section III, where we transmit at 10 GHz over 2000 km of SMF whose PMD and CD parameters are 0.1 ps/$\sqrt{\text{km}}$ and 17 ps/nm · km, respectively. Suppose CD is compensated using inline dispersion compensation fiber to within 5% error. From Section III, we have $2\pi|\beta_2|L_{\text{fiber}}R_s^2 = 8.5$ symbol intervals. By using (30), the length of the FSE that is required for 3/2-time oversampling is 15 taps, which is rounded to the nearest odd integer. Thus, the equalizer operation in (11) requires 60 complex multiplication per symbol at 8-b resolution. Achieving such performance would require a very large-scale integrated circuit with extensive pipelining and parallelization.

V. CONCLUSION

We have demonstrated the ability of an FSE to compensate for any linear channel impairment in a dually polarized optical system, including CD and any arbitrary amount of first-order PMD. We derived the optimal tap settings for an FSE based on the MMSE criterion, and we also evaluated the theoretical MSE performance. Our simulations showed that MMSE is a valid performance criterion despite the potential non-Gaussianity of

crosstalk and ISI. For NRZ, 33% RZ, 50% RZ, and 67% RZ pulses, we showed that the FSE is insensitive to sampling time errors and can correct an arbitrary amount of CD and first-order PMD with less than 2-dB power penalty if an oversampling rate of $M/K \geq 3/2$ is used in conjunction with a fifth-order Butterworth antialiasing filter. We showed that the amount of CD distortion that can be compensated by an FSE with N taps is approximately $|\beta_2|L_{\text{fiber}}R_s^2(M/K) \approx 0.15$ N, whereas the amount of first-order PMD DGD that can be compensated is $\tau_{\text{PMD}}M/K = NT_s$, where M/K is the oversampling ratio.

REFERENCES

[1] J. Wang and J. M. Kahn, "Performance of electrical equalizers in optically amplified OOK and DPSK systems," *IEEE Photon. Technol. Lett.*, vol. 16, no. 5, pp. 1397–1399, May 2004.

[2] D. Schlump, B. Wedding, and H. Bülow, "Electronic equalisation of PMD and chromatic dispersion induced distortion after 100 km standard fibre at 10 Gb/s," in *Proc. ECOC*, Madrid, Spain, 1998, pp. 535–536.

[3] F. Buchali and H. Bülow, "Adaptive PMD compensation by electrical and optical techniques," *J. Lightw. Technol.*, vol. 22, no. 4, pp. 1116–1126, Apr. 2004.

[4] R. Noé, D. Sandel, M. Yoshida-Dierolf, S. Hinz, V. Mirvoda, A. Schöpflin, C. Glingener, E. Gottwald, C. Scheerer, G. Fischer, T. Weyrauch, and W. Haase, "Polarization mode dispersion compensation at 10, 20, and 40 Gb/s with various optical equalizers," *J. Lightw. Technol.*, vol. 17, no. 9, pp. 1602–1616, Sep. 1999.

[5] H. Rosenfeldt, R. Ulrich, U. Feiste, R. Ludwig, H. G. Weber, and A. Ehrhardt, "PMD compensation in 10 Gb/s NRZ field experiment using polarimetric error signal," *Electron. Lett.*, vol. 36, no. 5, pp. 448–450, Mar. 2000.

[6] J. G. Proakis, *Digital Communications*, 3rd ed. New York: McGraw-Hill, 1995.

[7] R. D. Gitlin and S. B. Weinstein, "Fractionally spaced equalization: An improved digital transversal equalizer," *Bell Syst. Tech. J.*, vol. 60, no. 2, pp. 275–296, Feb. 1981.

[8] G. Ungerboeck, "Fractional tap-spacing equalizer and consequences for clock recovery in data modems," *IEEE Trans. Commun.*, vol. COM-24, no. 8, pp. 856–864, Aug. 1976.

[9] S. Qureshi, "Adaptive equalization," *Proc. IEEE*, vol. 73, no. 9, pp. 1349–1387, Sep. 1985.

[10] J. G. Proakis, "Adaptive equalization for TDMA digital mobile radio," *IEEE Trans. Veh. Technol.*, vol. 40, no. 2, pp. 333–341, May 1991.

[11] C. J. Nicol, P. Larsson, K. Azadet, and J. H. O'Neill, "A low-power 128-tap digital adaptive equalizer for broadband modems," *IEEE J. Solid-State Circuits*, vol. 32, no. 11, pp. 1777–1789, Nov. 1997.

[12] S. Tsukamoto, K. Katoh, and K. Kikuchi, "Unrepeated transmission of 20-Gb/s optical quadrature phase-shift-keying signal over 200-km standard single-mode fiber based on digital processing of homodyne-detected signal for group-velocity dispersion compensation," *IEEE Photon. Technol. Lett.*, vol. 18, no. 9, pp. 1016–1018, May 2006.

[13] S. Tsukamoto, K. Katoh, and K. Kikuchi, "Coherent demodulation of optical multilevel phase-shift-keying signals using homodyne detection and digital signal processing," *IEEE Photon. Technol. Lett.*, vol. 18, no. 10, pp. 1131–1133, May 2006.

[14] M. G. Taylor, "Coherent detection method using DSP for demodulation of signal and subsequent equalization of propagation impairments," *IEEE Photon. Technol. Lett.*, vol. 16, no. 2, pp. 674–676, Feb. 2004.

[15] K. P. Ho, "Generation of arbitrary quadrature-amplitude modulation signals using a single dual-drive modulator," in *Proc. IEEE/LEOS Workshop Adv. Modulation Formats*, San Francisco, CA, Jul. 2004, pp. 11–12.

[16] G. P. Agrawal, *Fiber-Optic Communication Systems*. New York: Wiley, 1997.

[17] J. M. Cioffi, G. P. Dudevoir, M. V. Eyuboglu, and G. D. Forney, "MMSE decision-feedback equalizers and coding—Part I: Equalization results," *IEEE Trans. Commun.*, vol. 43, no. 10, pp. 2582–2594, Oct. 1995.

[18] E. Ip and J. M. Kahn, "Power spectra of return-to-zero optical signals," *J. Lightw. Technol.*, vol. 24, no. 3, pp. 1610–1618, Mar. 2006.

[19] K.-P. Ho and J. M. Kahn, "Spectrum of externally modulated optical signals," *J. Lightw. Technol.*, vol. 2, no. 2, pp. 658–663, Feb. 2004.

[20] J. Winters, "Equalization in coherent lightwave systems using a fractionally spaced equalizer," *J. Lightw. Technol.*, vol. 8, no. 10, pp. 1487–1491, Oct. 1990.

[21] S. Fan and J. M. Kahn, "Principal modes in multimode waveguides," *Opt. Lett.*, vol. 30, no. 2, pp. 135–137, Jan. 2005.

[22] N. Amitay and J. Salz, "Linear equalization theory in digital data transmission over dually polarized fading radio channels," *Bell Labs Tech. J.*, vol. 63, no. 10, pp. 2215–2259, Dec. 1984.

Ezra Ip received the B.E. (Hons.) degree in electrical and electronics engineering from the University of Canterbury, Christchurch, New Zealand, in 2002 and the M.S. degree in electrical engineering from Stanford University, Stanford, CA, in 2004, where he is currently working toward the Ph.D. degree in electrical engineering.

In 2002, he was a Research Engineer at Industrial Research Ltd, New Zealand. He is currently with the Department of Electrical Engineering, Stanford University. His research interests include single-mode optical fiber communications, free-space optical communications, and nonlinear optics.

Joseph M. Kahn (M'90–SM'98–F'00) received the A.B., M.A., and Ph.D. degrees in physics from the University of California (UC), Berkeley, in 1981, 1983, and 1986, respectively.

From 1987 to 1990, he was at AT&T Bell Laboratories, Crawford Hill Laboratory, Holmdel, NJ. He demonstrated multigigabit-per-second coherent optical fiber transmission systems, setting world records for receiver sensitivity. From 1990 to 2003, he was with the Faculty of the Department of Electrical Engineering and Computer Sciences, UC, performing research on optical and wireless communications. Since 2003, he has been a Professor of electrical engineering at Stanford University, Stanford, CA. His current research interests include single- and multimode optical fiber communications, free-space optical communications, and MEMS for optical communications.

Prof. Kahn received the National Science Foundation Presidential Young Investigator Award in 1991. From 1993 to 2000, he served as a Technical Editor of the *IEEE Personal Communications Magazine.* In 2000, he helped found StrataLight Communications, where he served as Chief Scientist from 2000 to 2003.